AlGaN/GaN high electron mobility transistor with Al_2O_3+BCB passivation

Zhang Sheng(张 昇)[a)b)], Wei Ke(魏 珂)[b)†], Yu Le(余 乐)[a)b)], Liu Guo-Guo(刘果果)[b)], Huang Sen(黄 森)[b)], Wang Xin-Hua(王鑫华)[b)], Pang Lei(庞 磊)[b)], Zheng Ying-Kui(郑英奎)[b)], Li Yan-Kui(李艳奎)[b)], Ma Xiao-Hua(马晓华)[a)‡], Sun Bing(孙 兵)[b)], and Liu Xin-Yu(刘新宇)[b)]

[a)] *School of Advanced Materials and Nanotechnology, Key Laboratory of Wide Bandgap Semiconductor Materials and Devices, Xidian University, Xi'an* 710071, *China*

[b)] *Microwave Device and IC Department, Institute of Microelectronics, Chinese Academy of Sciences, Beijing* 100029, *China*

(Received 8 June 2015; revised manuscript received 23 July 2015; published online 12 October 2015)

In this paper, $A1_2O_3$ ultrathin film used as the surface passivation layer for AlGaN/GaN high electron mobility transistor (HEMT) is deposited by thermal atomic layer deposition (ALD), thereby avoiding plasma-induced damage and erosion to the surface. A comparison is made between the surface passivation in this paper and the conventional plasma enhanced chemical vapor deposition (PECVD) SiN passivation. A remarkable reduction of the gate leakage current and a significant increase in small signal radio frequency (RF) performance are achieved after applying Al_2O_3+BCB passivation. For the Al_2O_3+BCB passivated device with a 0.7 μm gate, the value of f_{max} reaches up to 100 GHz, but it decreases to 40 GHz for SiN HEMT. The f_{max}/f_t ratio (≥ 4) is also improved after Al_2O_3+BCB passivation. The capacitance–voltage (C–V) measurement demonstrates that Al_2O_3+BCB HEMT shows quite less density of trap states (on the order of magnitude of 10^{10} cm^{-2}) than that obtained at commonly studied SiN HEMT.

Keywords: AlGaN/GaN HEMT, Al_2O_3, BCB, passivation

PACS: 73.40.Ns, 76.61.Ey, 73.20.–r **DOI:** 10.1088/1674-1056/24/11/117307

1. Introduction

Many issues still exist in wide applications of AlGaN/GaN HEMT. One major problem is the electron trapping, which restricts the microwave output power and linearity. The traps are located mainly at the semiconductor surfaces/interfaces and in the GaN buffer layer. Deposition of a passivation layer mitigates the contribution from surface traps. PECVD SiN thin films are commonly used for surface passivation,[1,2] thus improving the performance of the device. However, the SiN passivation technique has faced some serious problems including: i) possible plasma-induced damages to the surface when PECVD is used to deposit SiN[3] films; ii) the contradiction between the current collapse suppression and higher leakage current;[4] iii) the mismatch with GaN makes lots of traps in the SiN, further leading to pinholes. SiN passivation may result in undesired device characteristics, such as higher gate leakage and lower cutoff frequency.

In recent years, some new methods to deal with the surface conditions and new passivation layer, such as Sc_2O_3,[5,6] SiO_2,[7] MgO,[8] AlN,[9,10] and Al_2O_3[11] have been used more frequently. In contrast to the conventional SiN passivation, Al_2O_3 thin film has more additional benefits,[12] such as a large band-gap (~8.9 eV), thermal stability (amorphous up to at least 1000 °C), a high breakdown field (5–10 MV/cm), and chemical stability against GaN, and thus it is a compelling candidate for AlGaN/GaN HEMT passivation.[7,13] For thermal ALD, water vapor is used as an oxidant and no plasma treatment is needed. Al_2O_3 deposited by thermal ALD has been demonstrated to have a low defect density, high uniformity, and nanometer scalability. In this paper, a 20-nm Al_2O_3 passivation layer is deposited on the AlGaN surface, and then heat cured benzo cyclo butane (BCB), which offers good thermal stability and chemical stability, is used to protect Al_2O_3 from being damaged and polluted.

2. Experiment

Figure 1 shows the cross section of AlGaN/GaN HEMT. The epitaxial layers were grown on SiC substrate by metal organic chemical vapor deposition (MOCVD) and the heterostructure consists of a 1.5-nm GaN cap layer, 17.6-nm $Al_{0.25}GaN$, 2-nm AlN, and GaN buffer layer. For the starting material considered here, the sheet resistance (R_{sq}) values as high as 272.4 Ω/sq and a Hall mobility of 2361 cm^2/V^{-s} are demonstrated at room temperature (300 K). The source-drain and gate length are 2.4 μm and 0.7 μm, respectively. The process for the GaN HEMT device follows the conventional steps: mesa isolation with N molecules, ohmic metallization with Ti/Al/Ni/Au (=200/1800/550/450±100 Å), annealing at 870 °C for 50 s by using rapid thermal annealing in nitrogen atmosphere, and it has a contact resistance as low as $\rho_c = 1.787 \times 10^{-5}$ Ω·cm^2. The gate metallization Ni/Au (100/3000 Å) is confirmed with electron beam lithog-

†Corresponding author. E-mail: weike@ime.ac.cn

‡Corresponding author. E-mail: xhma@xidian.edu.cn

© 2015 Chinese Physical Society and IOP Publishing Ltd

raphy. To investigate the influence of Al_2O_3+BCB passivation on HEMT, the substrate is split into two pieces which are passivated respectively with 200-nm SiN and 20-nm Al_2O_3. Then 2.7-μm BCB is deposited on the Al_2O_3 layer. Reference [13] gave the interface characteristics between Al_2O_3 and AlGaN/GaN in detail. In the present paper, we ultimately select a thickness of 20 nm, considering the vertical structure of the device and the practical coverage of Al_2O_3.

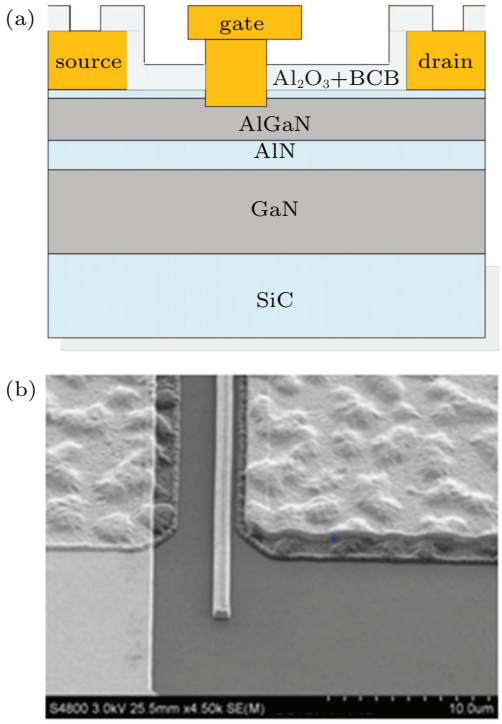


Fig. 1. (color online) (a) Cross section of AlGaN/GaN HEMT; (b) micrograph of T-gate.

3. Results and discussion

3.1. DC characteristics

We measure DC characteristics for the small gate width of the 50-μm periphery device by using an HP4155A semiconductor parameter analyzer. Figure 2(a) shows the transfer characteristics of the two devices before and after passivation at $V_{ds} = +6$ V. The peak transconductance (G_m) of an unpassivated device is 250 mS/mm and increases to 307 mS/mm after SiN passivation, and it increases to 301 mS/mm after Al_2O_3+BCB passivation. Figure 2(b) shows the IV characteristics. The maximum drain current density is 0.82 A/mm for the unpassivated device, it increases to 0.97 A/mm after SiN passivation, and it increases to 1.1 A/mm after Al_2O_3+BCB passivation. DC characteristics of devices increase significantly after passivation. In addition, it can be seen that the G_m, in a wide range, keeps a constant, indicating that the device with Al_2O_3+BCB passivation shows an outstanding linearity.

Another important parameter is the gate leakage current. In this case, the drain contact is biased at zero voltage and the

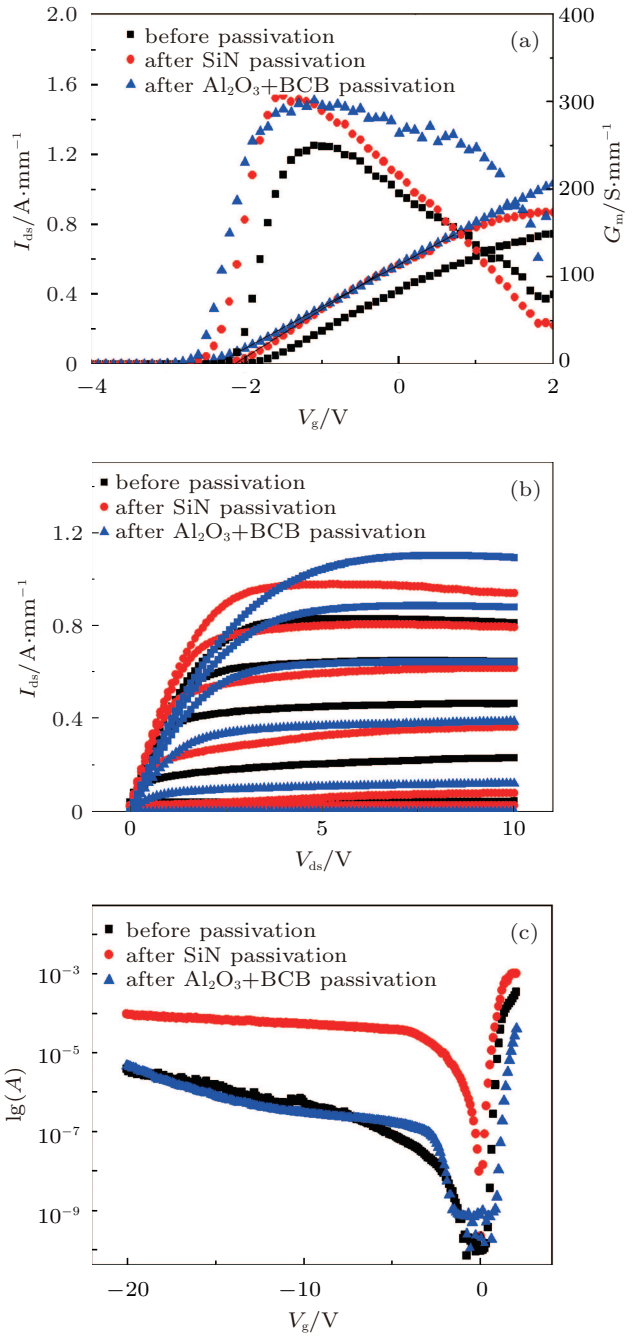


Fig. 2. (color online) (a) Transfer characteristics of transistors, (b) *I*–*V* characteristics of transistors, and (c) the gate leakage current of transistors.

gate is swept from 2 V to −20 V. Two samples after passivation present a significant difference as shown in Fig. 2(c). Negligible increase of the leakage current is found after device passivation with Al_2O_3+BCB, while the leakage current increases about one order of magnitude after SiN passivation. Besides, compared with the SiN passivation HEMT, the turn-on voltage of the Al_2O_3+BCB passivation HEMT increases slightly. The bigger the turn-on voltage is, the higher the reliability of the device is. It is considered that the suppression of the gate leakage current seems to come from the reaction of the AlGaN surface with oxygen from Al_2O_3.[14] The surface reaction removes the donor-like traps on the surface and makes

the current flow only through the 2DEG channel.[15] Here, the ideal factor of the Schottky contact n is also extracted. For Al_2O_3+BCB passivation and SiN passivation, $n = 1.87$ and 2.1, respectively. The smaller n is related to the low leakage current and the better surface quality.

3.2. RF characteristics

The S parameters of the two devices after passivation with a 50-μm gate width are measured as a function of frequency and bias by using an Agilent HP8510C Vector Network Analyzer. The corresponding current gain and maximum available gain (MAG) are shown in Figs. 3 and 4. The values of current gain cutoff frequency (f_t) are similar (about 20 GHz) for both devices. However, the maximum oscillation frequency (f_{max}) for the Al_2O_3+BCB passivation device is found to be much higher than that of the SiN passivation device. The f_{max}/f_t ratio ($\geq$4) changes significantly after Al_2O_3+BCB passivation. From these results, it is clear that an enhancement of small signal radio frequency (RF) performance can be achieved after Al_2O_3+BCB device passivation. We consider that the density of interface or surface states might be relevant to the RF performance of AlGaN/GaN HEMT and the improved RF performance indicates that Al_2O_3+BCB passivation contributes to reducing the surface states and is an excellent passivation technology.

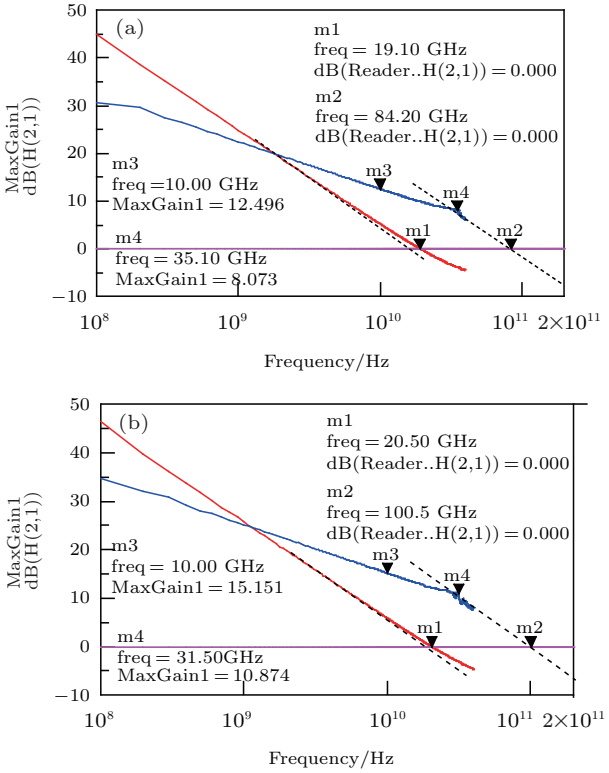


Fig. 3. (color online) Small-signal characteristics of Al_2O_3+BCB passivation HEMT. (a) $V_{ds} = 6$ V, $V_{gs} = -1.5$ V; (b) $V_{ds} = 28$ V, $V_{gs} = -1.5$ V.

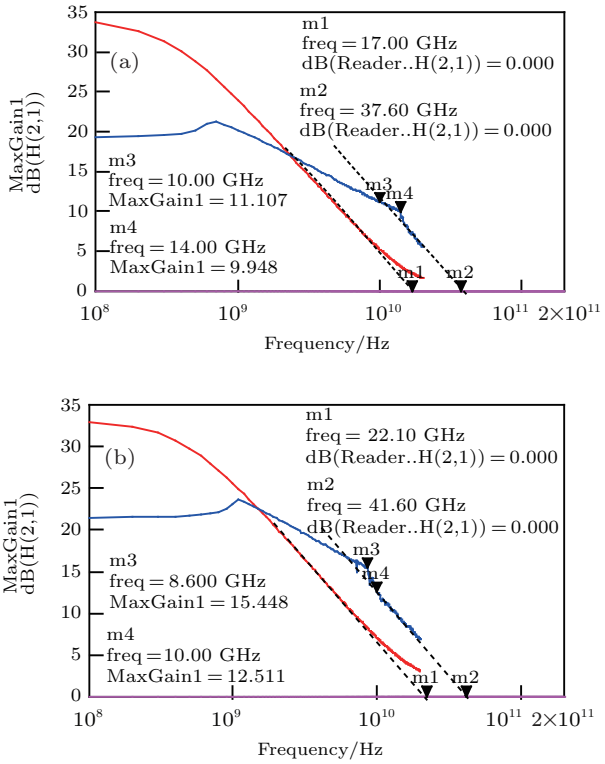


Fig. 4. (color online) Small-signal characteristics of SiN passivation HEMT. (a) $V_{ds} = 6$ V, $V_{gs} = -1.5$ V; (b) $V_{ds} = 28$ V, $V_{gs} = -1.5$ V.

Table 1. Small-signal characteristics of the two devices.

	V_{ds}/V	f_t/GHz	f_{max}/GHz	$Gain_{10GHz}$/dB	Knee freq/GHz
SiN	6	17.0	37.6	11.107	14.0
passivation	28	22.1	41.6	12.511	8.6
Al_2O_3+BCB	6	19.1	84.2	12.49	35.1
passivation	28	20.5	100.5	15.151	31.5

To further investigate the RF characteristics of the two devices, small-signal parameters are extracted using a 22-element equivalent circuit model as shown in Fig. 5. It can be found that the simulated data are in good agreement with the measured results, demonstrating the effectiveness of the parameter extraction. Obviously, there are little differences among the values of G_m, C_{gs}, and C_{gd} of the two devices, while there exists a significant difference between the two output resistance R_{ds} values. In general, R_{ds} depends on the current flowing through the buffer layer and indicates the quality of the buffer layer. In this paper, the only difference between the two devices is the passivation layer, and R_{ds} could be used to represent the surface and barrier layer, reasonably, implying that the low density of trapping (avoiding plasma-induced damage) causes the current flowing through barrier layer to decrease, and then the R_{ds} for Al_2O_3+BCB HEMT to increase. From the following equations:

$$f_T = \frac{g_m}{2\pi(C_{gs}+C_{gd})}, \tag{1}$$

$$f_{\max} \cong \frac{f_{\mathrm{T}}}{2\left(\left(\frac{R_{\mathrm{g}}+R_{\mathrm{i}}+R_{\mathrm{s}}}{R_{\mathrm{ds}}}\right)+2\pi f_{\mathrm{T}} C_{\mathrm{gd}} R_{\mathrm{g}}\right)^{1/2}}, \quad (2)$$

it follows that the f_{t} values of the two devices are substantially the same; and there is a 58.6% improvement in $f_{\max}$ for Al_2O_3+BCB HEMT. The $f_{\max}/f_{\mathrm{t}}$ ratio for Al_2O_3+BCB HEMT increases about twice, compared with that for the SiN HEMT. Namely, it could enhance the power and gain characteristics by making the Al_2O_3+BCB passivation for AlGaN/GaN HEMT work at a higher frequency, but unnecessarily by reducing the gate length. Furthermore, we believe that the different resistances R_{gdf} and R_{gsf},[16] related to the resistances of the gate-to-source and gate-to-drain diodes, are necessary to describe the gate leakage current conduction under the negative gate bias condition,[17] which is meaningful for AlGaN/GaN HEMT. The larger resistance indicates few surface traps and a better Schottky characteristic.

3.3. *C–V* measurement

In insulator/semiconductor systems, the electrical characteristics are greatly affected by some charges at the surface or within bulk materials, resulting from native or process-introduced defects. These charges can be determined by *C–V* measurement.

Surface trapped charges can usually be obtained from hysteresis *C–V* measurement by assuming that all other charges remain unchanged during device operation. The hysteresis *C–V* curves of the two devices shown in Fig. 6, demonstrate a flat band voltage shift (ΔV_{FB}) in the SiN HEMT and a negligible hysteresis in Al_2O_3+BCB HEMT. The shaded area represents the trapped charge quality, and the density (N_{t}) is calculated by using the following formula:

$$N_{\mathrm{t}} = \frac{\int_{V \geq V_{\mathrm{pinch-off}}}^{2V} \Delta C \, \mathrm{d}V}{q}, \quad (3)$$

where q is the electronic charge, $V_{\mathrm{pinch-off}}$ is the pinch-off voltage, and C is the capacitance per unit area. Among the studied devices, SiN HEMT demonstrates a larger trapped charge density of about 1.93×10^{11} cm^{-2}, and Al_2O_3+BCB passivation HEMT possesses better hysteretic characteristics with a trapped charge density of 2.1×10^{10} cm^{-2}. Additionally, so many charges can cause a serious reverse leakage current, featured by a decrease in reverse capacitance. From the curves in the inset of Fig. 6, Al_2O_3+BCB passivation exhibits good

Al_2O_3+BCB passivation	SiN passivation
device, $L_{\mathrm{g}} = 0.7$ μm, $W_{\mathrm{g}} = 50$ μm	
measured $f_{\mathrm{t}} = 20.5$	measured $f_{\mathrm{t}} = 22.1$
measured $f_{\max} = 100.5$	measured $f_{\max} = 41.6$
simulated $f_{\mathrm{t}} = 18.4$	simulated $f_{\mathrm{t}} = 21.5$
simulated $f_{\max} = 108.9$	simulated $f_{\max}$=47.9
intrinsic parameters	
$C_{\mathrm{gs}} = 127$ fF	$C_{\mathrm{gs}} = 98$ fF
$C_{\mathrm{gd}} = 5.5$ fF	$C_{\mathrm{gd}} = 7.2$ fF
$G_{\mathrm{m}} = 15.5$ mS	$G_{\mathrm{m}} = 14.6$ mS
$R_{\mathrm{i}} = 14.32$ Ω	$R_{\mathrm{i}} = 12.89$ Ω
$R_{\mathrm{ds}} = 1426.2$ Ω	$R_{\mathrm{ds}} = 904.5$ Ω
$R_{\mathrm{dgf}} = 24.0$ MΩ	$R_{\mathrm{dgf}} = 2.08$ MΩ
$R_{\mathrm{sgf}} = 31.228$ KΩ	$R_{\mathrm{sgf}} = 28.746$ KΩ

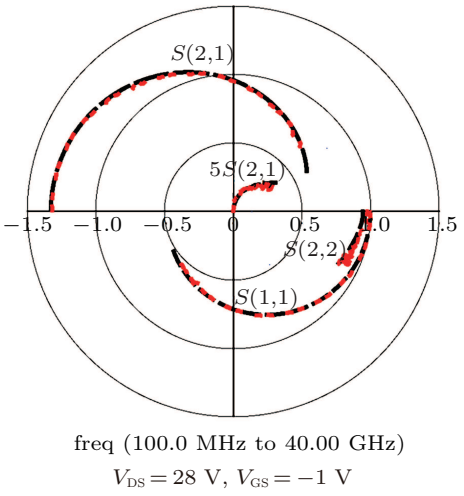


Fig. 5. (color online) Intrinsic parameters from determined S parameters.

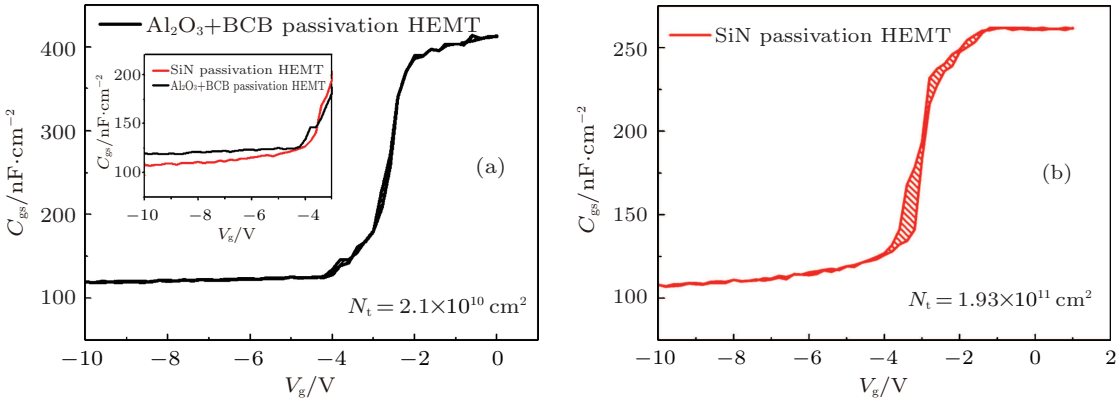


Fig. 6. (color online) (a) *C–V* characteristics of Al_2O_3+BCB passivation HEMT, and the reverse capacitance shown in the inset. (b) *C–V* characteristics of SiN passivation HEMT.

ability to block leakage current. The influence of surface trapping on the gate capacitance has been investigated by numerical simulation.[18] Briefly, the channel carrier under the gate is depleted in the off-state and only the fringe capacitance remains there. If there are many traps on the surface close to the gate, they serve as part of the gate and deplete the carriers under the surface, and thus reduce the capacitance.[19]

4. Conclusions

This paper elucidated the influence of Al_2O_3 deposited by thermal ALD on the AlGaN/GaN HEMT performance. An improvement in the gate leakage current characteristic and RF performance was obtained after device passivation with Al_2O_3+BCB as compared with the conventional PECVD SiN passivation. The C–V measurement indicates the promising application of Al_2O_3+BCB surface passivation material for GaN-based electronic devices. Especially, the increased f_{max}/f_t ratio indicates that the Al_2O_3+BCB passivation is an excellent potential for HEMT in high-frequency and high-power microwave applications.

References

[1] Koley G, Tilak V, Eastman L F and Spencer M G 2003 *IEEE Trans. Electron Devices* **50** 886

[2] Derluyn J 2005 *J. Appl. Phys.* **98** 054501

[3] Tang Z K, Huang S, Tang X, Li B K and Chen K J 2014 *IEEE Trans. Electron Dev.* **61** 2785

[4] Tan W S, Uren M J, Houston P A, Green R T, Balmer R S and Martin T 2006 *IEEE Electron Dev. Lett.* **27** 1

[5] Polyakov A Y, Smirnov N B, Govorkov A V, Danilin V N, Zhukova T A, Luo B, Ren F, Gila B P, Abernathy C R, Pearton S J and Onstine A H 2004 *J. Electrochem. Soc.* **151** G497

[6] Luo B, Johnson J W, Gila B P, Abernathy C R, Ren F, Pearton S J, Baca A G, Babiran A M, Wowchack A M and Chow P P 2002 *Solid-State Electron.* **46** 467

[7] Chevtchenko S A, Reshchikov M A, Fan Q, Ni X, Moon Y T, Baski A A and Morkoc H 2007 *J. Appl. Phys.* **101** 113709

[8] Gila B P, Hlad M, Onstlna A H, Frazier R, Thaler G T, Herrero A, Lambers E, Abernathy C R, Pearton S J, Anderson T, Jang S, Ren F, Moser N, Fitch R C and Freund M 2005 *Appl. Phys. Lett.* **87** 163503

[9] Sen H, Qimeng J, Shu Y, Chun H Z and Chen K J 2012 *IEEE Electron Dev. Lett.* **33** 516

[10] Sen H, Qimeng J, Shu Y, Zhi K T and Chen K J 2013 *IEEE Electron Dev. Lett.* **34** 193

[11] Ye P D, Yang B, Ng K K, *et al.* 2004 *IEEE Lester Eastman Conference on High Performance Devices* 4–6 167–172

[12] Yue Y Z, Hao Y, Zhang J C, Feng Q, Ni J Y and Ma X H 2008 *Chin. Phys. B* 17 1674

[13] Mizue C, Hori Y, Miczek M and Hashizume T 2011 *J. Appl. Phys.* **50** 021001

[14] Meyer D J 2008 *CS MANTECH Conference* 13.4 14–17

[15] Hong S K 2008 *Electronics Lett.* **44** 1091

[16] Berroth M and Bosch R 1991 *IEEE Trans. Microw Theory Tech.* **39** 224

[17] Qian F, Jacob H L and Hadis M 2010 *Proc. IEEE* **98** 1140

[18] Takatani S and Chen C D 2009 *Proc. IEEE CSIC Symp. Tech. Digest.* 137

[19] Takatani S and Chen C D 2011 *IEEE Trans. Electron Dev.* **58** 4301